AIMS Biophysics, 4(3): 451-464.
DOI: 10.3934/biophy.2017.3.451
Received: 20 January 2017
Accepted: 22 June 2017
Published: 30 June 2017

http://www.aimspress.com/journal/biophysics

Research article

In-situ AC electroosmotic and thermal perturbation effects for wide range of ionic strength

Reza Hadjiaghaie Vafaie [1,*] and Aysan Madanpasandi [2]

[1] Department of Electrical Engineering, Microsystem Research Group, University of Bonab, Bonab 5551761167, Iran
[2] Department of Electrical Engineering, Urmia University, Urmia 5756151818, Iran

* **Correspondence:** Email: reza.vafaie@bonabu.ac.ir; rzvafaiee@gmail.com; Tel: +989144012352.

Abstract: AC electrokinetic flow is promising in designing microfluidic chips for manipulation of biological and chemical samples toward clinical diagnostics. Four pieces of electrodes are optimized to enhance mixing effect inside a straight microchannel. In this research, the mixing dependency on the ionic strength of solutions is investigated. AC electroosmotic secondary flow is responsible for the mixing at low ionic strength ($\sigma < 5$ mS m^{-1}), whereas AC electrothermal secondary flow is proposed to mix high conductive mediums ($\sigma > 5$ mS m^{-1}). The electrode-electrolyte impedance analysis is employed to facilitate the in-situation mixing process by choosing appropriate electrical excitation parameters for the electrodes.

Keywords: ac electroosmotic; ac electrothermal; chaotic regime; microfluidic; electric conductivity

1. Introduction

The successful progress displayed in microelectronic industry has motivated the researchers in wide variety of fields to employ the concept of integration into fluid mechanics [1] and biological engineering [2,3,4] with the hope of cost-effectiveness and high performance enhancement. The low velocity and small scales cause very low Reynolds number fluid. Micro-scale disturbance and mixing process are highly challengeable issues in preparation step for bioprocess and Lab-on-a-Chip (LOC) analysis. Due to very low Reynolds number in microscale, the mixing effect is completely troublesome [5] (equation (1)).

$$\mathrm{Re} = \rho u l / \mu. \quad (1)$$

Where, ρ is the fluid density, u is the velocity vector, μ is the fluid dynamic viscosity and l is the characteristic length of microchannel. The viscose effect is dominant factor in micro-devices ($Re < 1$) and molecular diffusion is the main transport phenomena for mixing [5]. Rapid micromixing can be classified into passive and active micromixers [5]. The passive types enhance the fluids mixing effect by utilizing asymmetric channel geometry like serial lamination [6] and Zigzag shaped mixer [7]. In contrast to passive types, active micromixers increase the interfacial area between the fluids by using an external force such as magnetic [8], ultrasonic [9], and thermal [10] forces.

In past two decades, electrokinetic mechanism has been employed to mix fluids in microchannels. AC electroosmotic (ACEO) flow is more efficient for generating distribution effects. If a tangential electric field is applied to a fluid medium, the charges in the Electrical Double Layer (EDL) between the surface and the fluid, experience a significant force. EDL charges' movement pulls the fluid along the channeland generates ACEO flow [11]. Biddiss and et al. declared that applying a time-varying periodic electric field to the electrodes generates a chaotic regime and enhances mixing performance [12]. Electrokineticly driven (100 V/cm, 2 Hz) mixing effect was achieved by using a switched DC field to induce instability effects inside a microchannel [13]. A time-dependent external electric field is applied to generate secondary flows around internal obstacles in a microchannel [14]. Chen and Cho [15] designed a micromixer by employing chaotic regime. The oscillating electric potentials were derived by using a Duffing-Holmes chaos system. Vafaie et al. [4] presented a high throughput AC electroosmotically driven micromixer. The electrodes were covered by a thin insulator material in order to eliminate electrode degradation and unwanted electrochemical effects.

AC electroosmotic mechanism relies on the formation of EDL and thickness of EDL is dramatically related to the electrical conductivity of fluid mediums. It should be noted that high ionic strength buffers and solutions are very conventional in biological and immunoassay applications [16,17]. Therefore, EDL layer collapses in high conductive mediums and the electroosmotic flow loses its efficiency [18]. In contrast to ACEO, the AC Electrothermal (ACET) flow is remarkably efficient for high ionic strength fluids [19]. ACET flow was investigated to improve the binding efficiency of on-chip immunoassay biosensors [18]. ACET mechanism was also studied as an accompanying phenomenon in Di-electrophoresis particle manipulation [20]. AC field electrodes and DC-heating element were arranged as a method for ACET micro-pumping [21]. Most recently, Vafaie et al. [2] have experimentally investigated the ACET mechanism for bi-directional pumping of high conductive solutions. Vafaie and Ghavifekr [22] have presented a novel electrode engineering array for on-chip fluid manipulation by using ACET flow.

In this research, AC electroosmotic and AC electrothermal mixing process are investigated for wide range of ionic strength fluids which can be very helpful for in situ applications. The ACEO flows are employed to the electrode structures to enhance the mixing effect in low ionic strength and also ACET flows are applied to the same electrodes in order to mix high ionic strength mediums. A set of numerical studies is run to investigate the multi-physic ACEO and ACET flow effect on mixing efficiency.

2. Materials and Method

By considering a pair of side by side electrodes and applying a time-dependent electric field to the electrodes, two important mechanisms can be occurred. When the frequencies of the applied electric field and the medium charging ($\tau_q^{-1} = \sigma/\varepsilon$) are in the same range, the counter ions do not have enough time to completely screen the electrodes surface. A part of electric field is consumed for screening effect and the other part is dropped over the fluid medium (Figure 1A). The inner portions of EDL on the electrodes charge more rapidly than the outer portions. In this case the electrodes are partially screened and a tangential force causes to induce an ACEO flow from the screened portion towards the unscreened portion. It should be noted that the generated ACEO flow is independent of the sign of the applied electric potential. For very high actuation frequencies, there is not enough time for the ions to do screening effect and the entire electric field is dropped over the fluid medium (Figure 1B). This effect leads to locally temperature rise inside the channel. Based on Joule's law ($W = \sigma E^2$) the generated temperature increment is dependent on the fluid ionic strength [19].

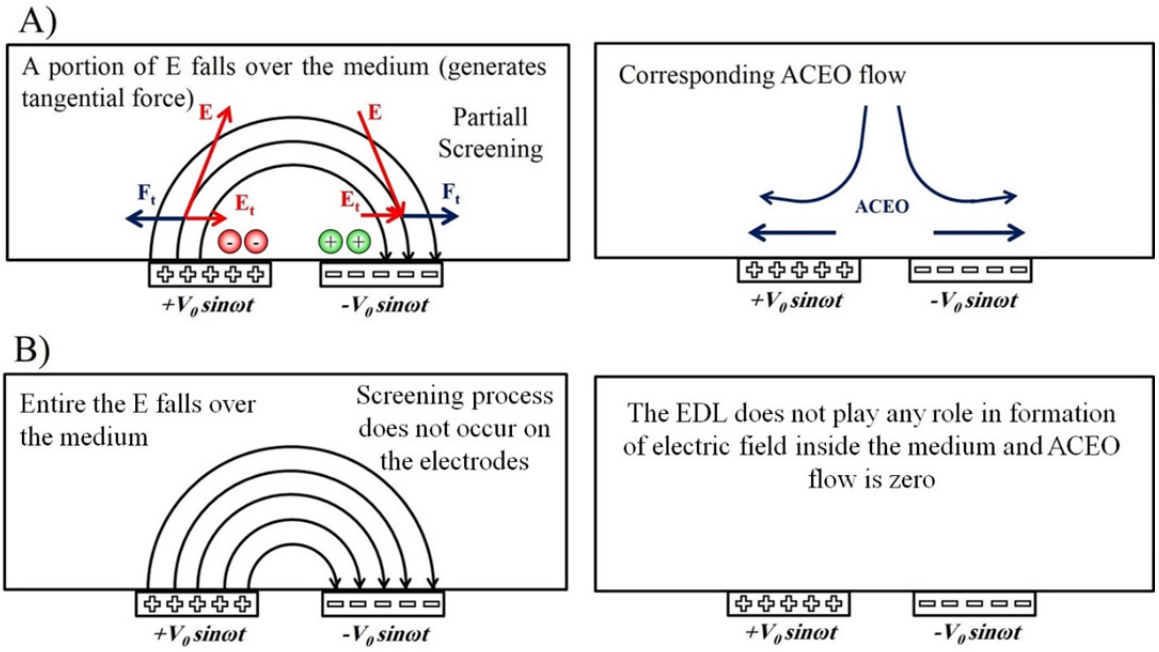

Figure 1. Electrokinetic mechanism; (A) AC electroosmotic flow for low ionic strength mediums, (B) AC electrothermal flow for high conductive mediums.

2.1. Theory

The governing equations for the ACEO and ACET flows in order to mix wide range of ionic strength are described as follows:

2.1.1. AC Electroosmotic theory

According to ACEO physical equation, a multi-physics coupled problem should be analyzed which includes fluid mechanics, electric field and Convection-Diffusion theory. Incompressible

Navier-Stokes equation (equation (2)) and continuity equation (equation (3)) solve the fluid motion inside the channel [23].

$$\rho\left[\frac{\partial \overline{u}}{\partial t}+\vec{u}\nabla\overline{u}\right]+\nabla p-\mu\nabla^2\vec{u}=\underbrace{f_{Bulk}}_{\rho_e\vec{E}}. \tag{2}$$

$$\nabla\overline{u}=0. \tag{3}$$

Where, p is the pressure in the micro channel, ρ_e is the electric charge density, and E is the generated electric field in micro channel.

A thin layer of EDL exists as the electrode-fluid medium interface, the characteristic thickness of electric double layer can be estimated by Debey length, λ_D:

$$\lambda_D=\sqrt{\varepsilon k_b T \Big/ 2n_i^0 z_i^2 e^2}. \tag{4}$$

Where, k_b is the Boltzmann constant, T is temperature, ε is dielectric constant of fluid medium, n_i^0 is bulk concentration of ion i, z_i is the valance of ion i and e is initial charge. The electric double layer thickness at low conductive mediums is typically about 10 nm.

The interaction between electrical double layer (EDL) and excess ions results in the electrical driving force which can be expressed by equation (5):

$$\overline{E}=-\nabla V\ . \tag{5}$$

Where V is the applied electric potential. In this case, the counter-ions in EDL experience a tangential force by imposing a time-varying electric field.

As a result, the charges' movement pulls the fluid inside the channel and generates a secondary flow. ACEO velocity (u) is approximated by Helmholtz-Smoluchowski equation (equation (6)) [24]. The effect of ACEO flow is considered as slip flow velocity at the edge of electric double layer. Therefore, the slip flow velocity boundary conditions can be considered by Incompressible Navier-Stokes for fluid motion inside the channel.

$$u=-\varepsilon_0\varepsilon_r\zeta\vec{E}\Big/\mu. \tag{6}$$

Where, ε_0 is the dielectric permittivity of vacuum, ε_r is the relative permittivity of the fluid, ξ is the electrokinetic zeta potential.

2.1.2. AC Electrothermal theory

In this section, the governing physical equations of the ACET mixing are described. By dropping an electric field over the high ionic strength mediums, temperature increases and also temperature gradients field is generated inside the channel. The generated temperature rise can be estimated by heat balance equation [25]:

$$\rho c_p\, u.\nabla T+\rho c_p\frac{\partial T}{\partial t}=k\nabla^2 T+\sigma|E|^2 \tag{7}$$

Where, T is the temperature, c_p is the specific heat and k is the thermal conductivity of medium. Generated temperature gradients cause gradients in electric properties (σ as electric conductivity and ε as electric permittivity). For an aqueous solution, equations (8) and (9) can be employed to demonstrate the temperature dependencies of σ and ε [26].

$$\sigma(T) = \sigma(T_0)(1 + \beta(T - T_0)), \quad \beta = \frac{1}{\sigma(T_0)}(\frac{\partial \sigma}{\partial T})\Big|_{T_0} = 2\%/K \tag{8}$$

$$\varepsilon(T) = \varepsilon(T_0)(1 + \alpha(T - T_0)), \quad \alpha = \frac{1}{\varepsilon(T_0)}(\frac{\partial \varepsilon}{\partial T})\Big|_{T_0} = -0.4\%/K \tag{9}$$

Where, T_0 is ambient temperature and the time-averaged ACET force per unit volume can be written as [27]:

$$\begin{gathered} < F_{ET} >= \frac{1}{2}.\frac{\varepsilon(\alpha - \beta)}{1 + (2\pi f\varepsilon/\sigma)^2}(\nabla T.E)E - \frac{1}{4}\varepsilon\alpha|E|^2\nabla T \\ \alpha = (\partial\varepsilon/\partial T)/\varepsilon \ ; \ \beta = (\partial\sigma/\partial T)/\sigma \\ \textit{for aqueous solution}: < F_{ACET} >= \underbrace{-0.012\nabla T.\frac{\varepsilon|E|^2}{1 + (\omega\tau)^2}}_{\textit{Colombic Force}} + \underbrace{0.001\nabla T.\varepsilon|E|^2}_{\textit{Dielectric Force}} \end{gathered} \tag{10}$$

Where, $\omega = 2\pi f_c$ is the angular frequency of AC electric field and $\tau = \varepsilon(T_0)/\sigma(T_0)$ is the charge relaxation time of medium. When $\omega_\tau << 1$, the columbic force is dominant to the dielectric force. However, for $\omega_\tau >> 1$, the dielectric force is dominant. The induced AC Electrothermal flow F_{ACET}, increases bulky fluid motion inside the channel. For high ionic strength fluids, the thickness of EDL is very low ($\lambda_D \approx (\varepsilon/\sigma)^{0.5}$), also the ACEO flow is completely negligible for applied frequencies above 100 kHz [28]. Therefore, exciting the electrodes by ACET flow over a high ionic strength fluid medium is proposes in order to generate high efficient local Joule heating effects. The generated ACET secondary flow is highly applicable for mixing effect. The electric field inside the channel is solved to calculate the ACET bulk flow. In addition, heat balance equation is solved to calculate the generated temperature increase and temperature gradient. In ACET driving case, the governing equations of fluid flow inside the channel is estimated as follows [2]:

$$\rho\left[\frac{\partial \bar{u}}{\partial t} + \vec{u}\nabla\bar{u}\right] + \nabla p - \mu\nabla^2\vec{u} = \underbrace{f_{Bulk}}_{F_{ACET}}. \tag{11}$$

2.1.3. Concentration field

A sample solution is often tested by a reagent in biological and chemical analysis. Two solutions should be mixed completely to make a possible test process. Micron scale mixing relies mainly on diffusion due to the laminar behavior at low Reynolds numbers and the mixing rate is determined by the flux of diffusion j [28]:

$$j = -\frac{dc}{dx} \tag{12}$$

Fast mixing time is achievable by decreasing the mixing path and increasing the interfacial area. The diffusive/convective transport of the solute in these concepts is governed by the transport equation as follows [28]:

$$\frac{\partial C}{\partial t} + u\frac{\partial C}{\partial x} + v\frac{\partial C}{\partial y} = D(\frac{\partial^2 C}{\partial x^2} + \frac{\partial^2 C}{\partial y^2}). \tag{13}$$

Where, C is the fluid species concentration and D is the diffusion coefficient of the buffer and sample. u and v are the velocity components in x- and y-*axis*, respectively. The concentration of fluid A and B are described by 1 and 0 mol m^{-3}, respectively.

2.2. Design

Mixing effect in a straight microchannel is investigated where four pieces of electrodes are embedded in the side walls of channel. The electrodes are excited by an appropriate electric field to generate ACEO and ACET fluid motions. Nanoscale solution and sample fluids are inserted inside the channel through inlets A and B. The proposed geometrical design is visualized in Figure 2 and the dimensions are assigned in accordance with Table 1. It assumes that the fluids have been previously pumped by a micropump which has the initial velocity of U_0. It should be noted that geometrical dimensions are optimized by Taguchi optimization method [29].

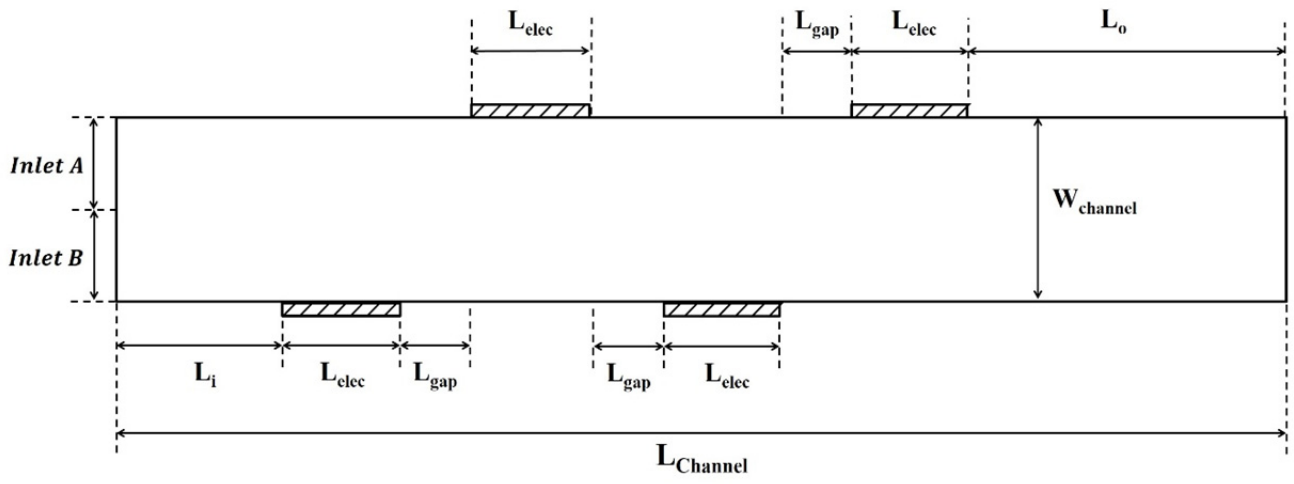

Figure 2. Schematic view of geometrical parameters of the micro-mixer (including microchannel, electrodes, inlets and outlet).

Table 1. Geometry parameters in the simulation model.

Symbol	Description	Value (μm)
$W_{Channel}$	Microchannel width	60
$L_{Channel}$	Microchannel length	400
L_{elec}	Electrode Width	40
L_{gap}	Gap between the electrodes	20
L_i	Distance between the inlet and the first electrode	60
L_o	Distance between the last electrode and the outlet	120

2.3. Initial/boundary conditions

In current model, the laminar flow is considered due to the low velocity and small length scale characteristic. The proposed system is able to mix working fluids with wide range of ionic strength inside the straight channel. The mean velocity of the initial fluid is U_0 and the pressures at the two ends of the channel have been considered as zero. In addition, the pressure gradient is set to be zero at the channel walls, considering no flux across the walls. The microchannel's walls are assumed to be smooth and the effect of surface roughness can be neglected [4]. Aqueous solutions A and B are taken into the channel with concentrations of 1 and 0 [mol m^{-3}], respectively. It assumes that the variation in the fluid concentration does not alter the density and viscosity of solutions [28].

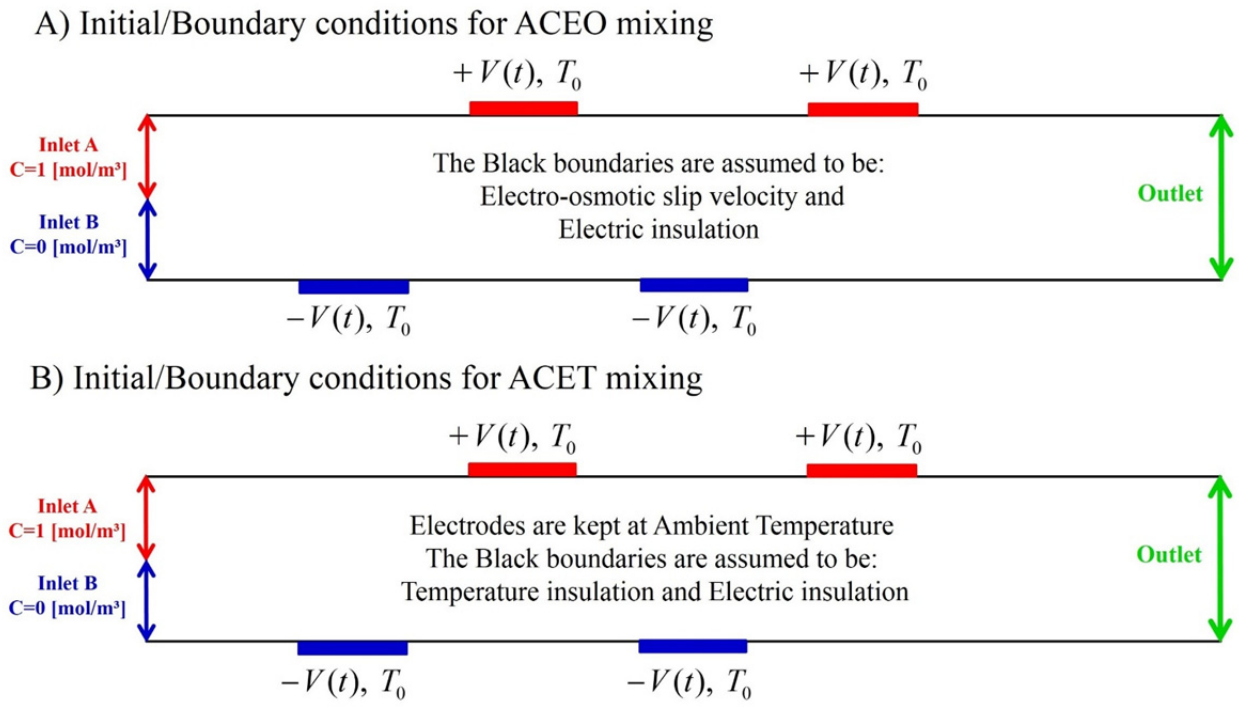

Figure 3. Initial and boundary conditions; (A) for ACEO mixing, (B) for ACET mixing.

Figure 3 summarizes some of the Initial/boundary conditions for the fluid mechanic including concentration, temperature and electric fields. Physical properties of electrolyte solutions and exciting parameters are assigned in accordance with Table 2. The electrodes are excited by an

appropriate electric potential to generate ACEO and ACET secondary flows. As a result, the species mixing process is induced by interaction between the primary steady flow and the secondary ACEO/ACET oscillating flow. For low ionic strength mediums (below 50 mS/m), the electrode pieces are excited by low frequencies (i.e. f_c from 100 Hz up to 20 kHz. In this case, the EDL is thick enough and ACEO flow is generated inside the channel [30]. Therefore, electroosmotic slip boundary conditions are applied to the side walls (Figure 3A) and the ζ potential effect is determined by slip boundary conditions. The slip velocity is proportional to the electric field intensity, the electric field decays exponentially away from the electrodes. It should be noted that the Joule heating and temperature increment are completely negligible for low ionic strength mediums.

Table 2. Material properties of solution.

Symbol	Description	Value
U_0	Initial pumped velocity	0.1 mm s^{-1}
ρ_m	Viscosity of fluid	1×10^{-3} N S m^{-2}
μ	Density of fluid	10^3 kg m^{-3}
σ	Electric conductivity of fluid	1 mS m^{-1} to 1 S m^{-1}
ε_r	Dielectric constant of fluid	80.2
ε_0	Vacuum permittivity	8.854×10^{-12} F m^{-1}
V_0	Amplitude of electric potential	1 Volt for ACEO mixing 7 Volts for ACET mixing
f_c	Frequency of electric signal	20 Hz–20 kHz for ACEO mixing 100 kHz–1 MHz for ACET mixing
c_p	Heat capacity of fluid	4.184 kJ $(kg\ K)^{-1}$
k	Thermal conductivity of fluid	0.598 W $(m\ K)^{-1}$
$T_{ambient}$	Ambient temperature	273.15 K
$C_{Fluid\text{-}A}$	Species Concentration of Fluid A	1 mol m^{-3}
$C_{Fluid\text{-}B}$	Species Concentration of Fluid B	0 mol m^{-3}
D	Diffusion coefficient	2×10^{-11} m^2 s^{-1}

For high conductive mediums (i.e. above 50 mS/m), the entire electric field is dropped over the fluid medium by exciting the electrodes at high frequencies (f_c from 100 kHz up to 1 MHz). The thermal properties of working fluid and silicon substrate are very important for ACET mixing process. It should be noted that silicon substrate is a good thermal conductor and pulls the generated temperature down onto the solid surface. As shown in Figure 3B, the temperature of the electrodes' surface and inlet are kept at ambient temperature (273.15 K). Outlet boundary condition is set as convective heat flux and thermal insulation boundary conditions are applied elsewhere. Thermal properties of biological buffer with various ionic strength have been chosen as working fluid in this study.

3. Results and Discussion

A set of Finite-Element-Method (FEM) simulation is run with COMSOL Multiphysic Software to investigate both the ACEO and ACET flow effects on mixing performance. A straight microchannel is designed and the simulation setup is built following the procedures outlined in Material and Methods section.

3.1. Impedance analysis

The electrode-electrolyte behavior is modeled by electrical lumped circuit model. As shown in the equivalent circuit (Figure 4), R_{Lead} exhibits resistivity of the electrode material, C_{EDL} represents the AC charging effect at electrode-electrolyte interface which treats as capacitor. Functioning of C_{EDL} is not ideal and performs like Constant Phase Element (CPE) as explained by Jorcin et al. [31]. The bulk fluid treats as resistor ($R_{Solution}$). DC/AC electric current passes through $R_{Solution}$ and increases the fluid's temperature according to Joule's law. $C_{Dielectric}$ indicates direct dielectric coupling between the electrodes which performs at very high frequencies where medium polarization occurs. Based on the applied electric field frequency and electrical properties of the electrolyte (σ and ε_r), the behavior of the equivalent circuit is variable. For low ionic strength mediums (below 50 mS/m), the C_{EDL} impedance is much more than $R_{Solution}$. Therefore, ACEO flow is dominant and most of the voltage drops across the EDL and the lumped circuit model displays capacitive characteristic for system. By increasing the frequency (i.e 100 kHz up to 1 MHz), the impedance of C_{EDL} decreases and most of the voltage drops over the fluid medium. As a result, higher current passes through the $R_{Solution}$ and thermal effect is dominant. In this case, the equivalent circuit model exhibits most resistive characteristic. However, for much higher frequencies (well above 10 MHz), the impedance of $C_{Dielectric}$ becomes dominant and the whole system displays characteristic again. These results are confirmed by impedance analysis for different ionic strength mediums. For 8 mS/m working fluid the impedance analysis results in 1.52 kΩ magnitude and –75.3° phase angle at 100 Hz. It means that the characteristics of the system are mostly capacitive and the impedance of C_{EDL} is more dominant than impedance of $R_{Solution}$. Impedance analysis for 0.1 S/m fluid medium results in 36.8 Ω magnitude and –4.7° phase angle at 200 kHz. Therefore, the $R_{Solution}$ is responsible for power generation and the corresponding ACET flow.

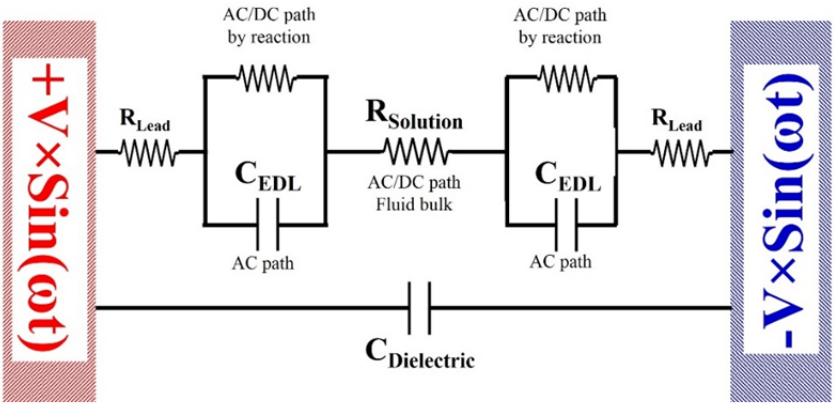

Figure 4. Lumped circuit model for electrode-electrolyte interaction.

3.2. *Ac electroosmotic*

For low ionic strength mediums, the electrodes are excited in ACEO mode by an electrical signal which its amplitude and frequency are +/–1 Volt and 20 Hz–20 kHz, respectively (presented in Table 2). Under these conditions, an efficient electroosmotic secondary flow is generated within the EDL at the side walls. As a result of ACEO effect, the fluid flows from upper electrode toward the electrode located at the down side and vice versa. The interaction between the primary pumped flow and secondary induced ACEO flow causes a perturbation inside the microchannel. Both the species concentration distribution and species concentration profile at the outlet of channel are illustrated in Figure 5. When the electrodes are not excited, the species profile has a smooth distribution (i.e. t = 0 sec) and it indicates a poor mixing effect. By exciting the electrodes (i.e. t > 0 sec) in ACEO mode, both A and B species are perturbed by oscillating secondary flow.

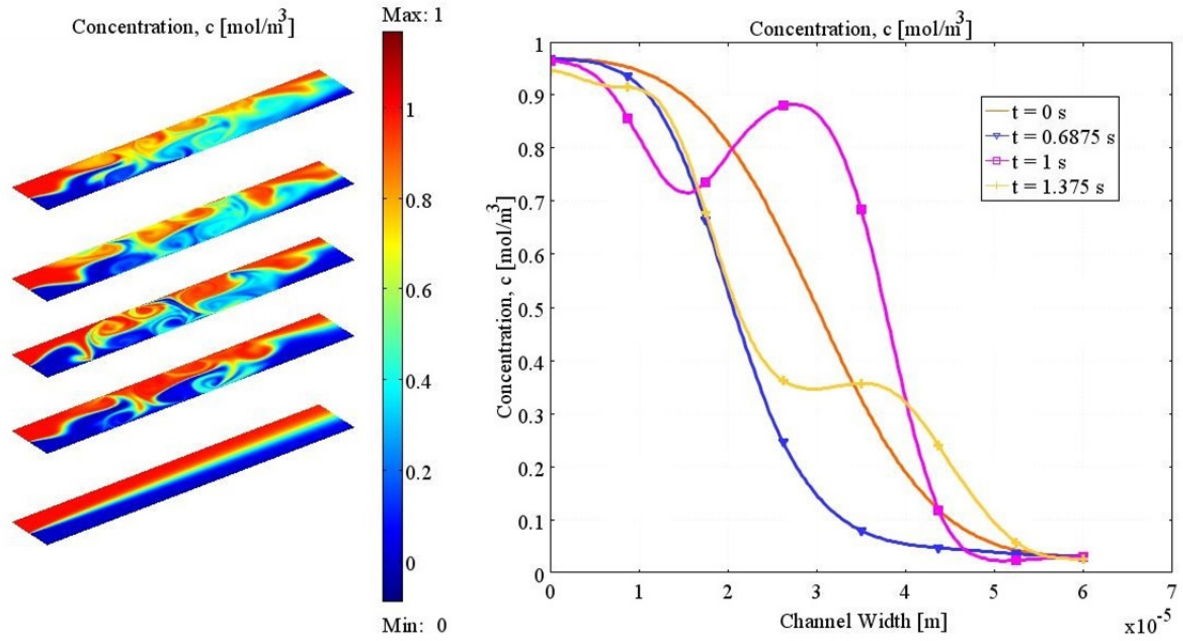

Figure 5. ACEO mixing; distribution of the species and concentration plot at the outlet of the channel in an electrolyte of conductivity 2 mS m^{-1} by applying an electric signal (+/–1 Volt, 200 Hz), t = 0 sec. corresponds to non-secondary flow.

3.3. *Ac electrothermal*

The mixing process is investigated for high ionic strength mediums under the influence of ACET flow (ACET excitation parameters are shown in Table 2). Figure 6 depicts the ACET flow effect on both the species distribution and concentration profile at the outlet of the microchannel. For t = 0 sec (i.e. without ACET flow), poor mixing of the species is occurred only by molecular diffusion phenomenon at the interface between the solutions A and B. By applying the ACET flow, the interfacial area between the two species is increased and as a result, both fluids are perturbed. The secondary ACET flows enhances the mixing effect by stretching, folding and breaking the fluids

up. By passing more time, the species concentration at the outlet of the mixing channel approaches to 0.5 mol m^{-3}.

It should be noted that dropping an electric field over the fluid medium, generates temperature rise inside the channel. For an applied electric field with constant amplitude, both the temperature rise and ACET force increase by increasing fluid conductivity. The maximum temperature rise of 2.86 K is observed for 0.1 S/m medium.

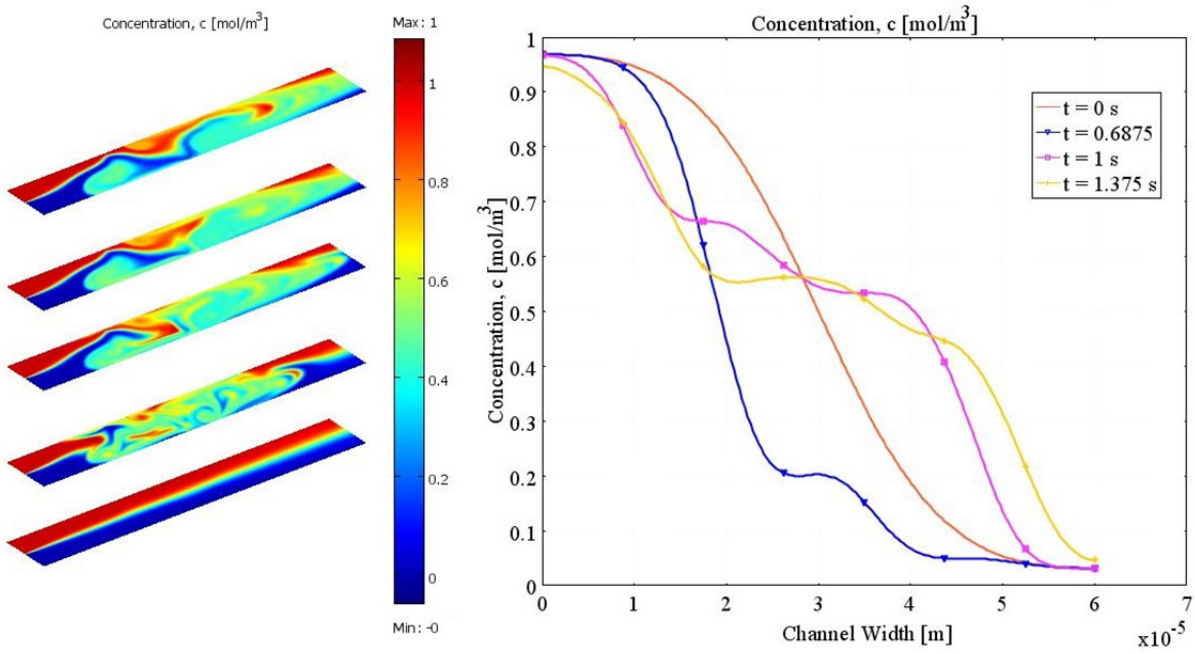

Figure 6. ACET mixing; distribution of the species and concentration plot at the outlet of the channel in an electrolyte of conductivity 1 S m^{-1} by applying an electric signal (+/–7 Volt, 200 kHz), t = 0 sec. corresponds to non-secondary flow.

3.4. Mixing efficiency

Based on the FEM-Analysis for four pieces of embedded electrodes, mixing process is enhanced by inducing ACEO flow over the low ionic strength medium. Furthermore, ACET driving flow is efficient for high conductive mediums. These flows are able to generate secondary flow associated with stretching and folding effects. T_0 evaluates mixing quality, the efficiency Q at any cross-section of the channel can be quantified by the following equation [32].

$$Q = [1 - \frac{\int_A |C - C_\infty| \, dA}{\int_A |C_0 - C_\infty| \, dA}] \times 100\ \%. \tag{14}$$

Where, C is the species concentration across the channel width, C_{oo} is the species concentration in the completely mixed state (C_{oo} = 0.5), and C_0 is species concentration in the completely unmixed condition (C_0 = 0 or 1). Figure 7 illustrates the mixing quality for both the ACEO and ACET mixers.

Figure 8 depicts the mixing quality for wide range of ionic strength medium (from 1 mS m^{-1} up to 1 S m^{-1}). It should be noted that the mixing quality improves by (a) using more electrode arrays and (b) increasing the amplitude of electric potential.

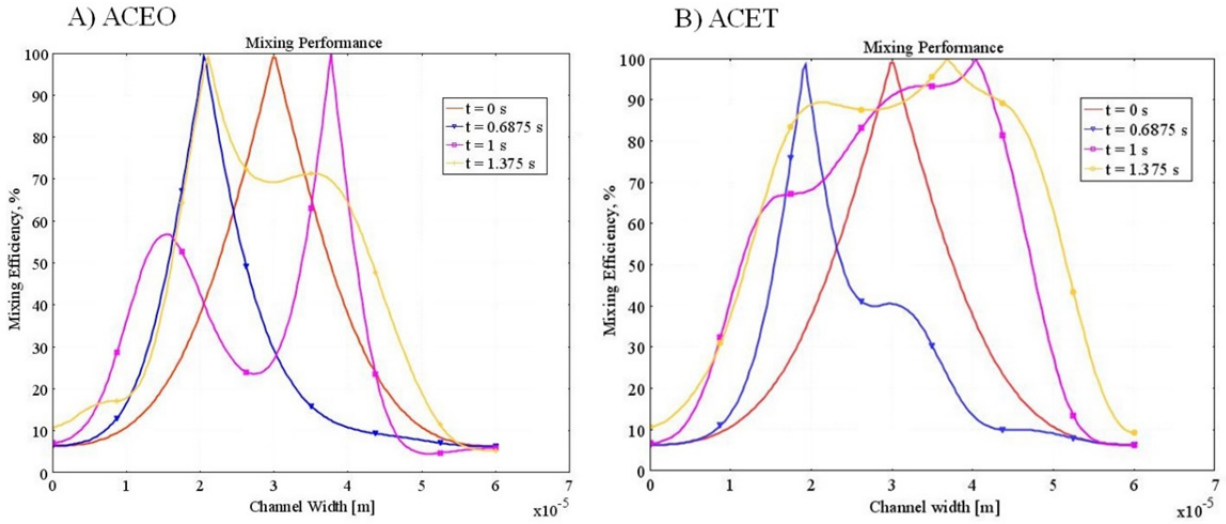

Figure 7. Mixing performance for different times; (A) ACEO driven flow, in an electrolyte of conductivity 2 mS m^{-1} by applying an electric signal (+/–1 Volt, 200 Hz), (B) ACET driven flow, in an electrolyte of conductivity 0.1 S m^{-1} by applying an electric signal (+/–7 Volt, 200 kHz).

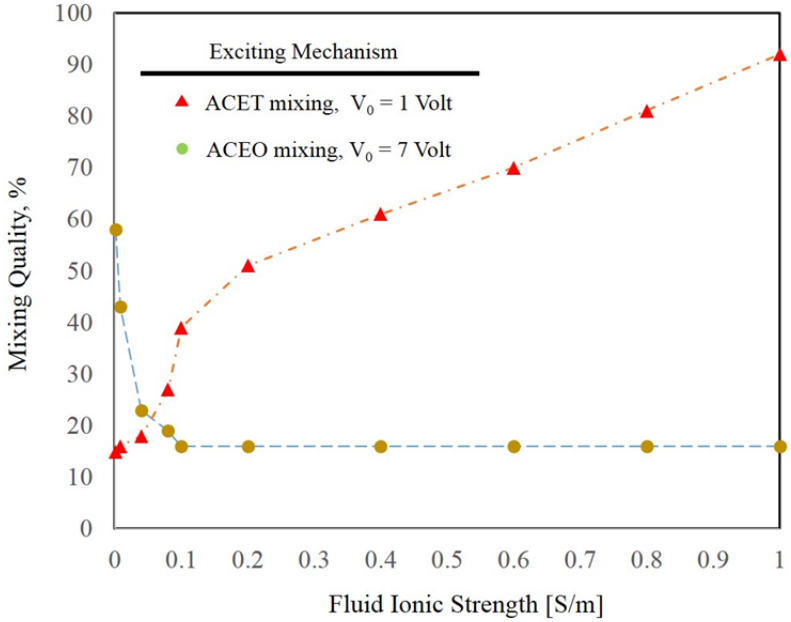

Figure 8. Ionic strength effect on mixing quality of AC Electrothermally-driven and AC Electroosmotically-driven mixers.

4. Conclusions

In this research, a miniaturized channel and four pieces of electrodes were optimized to investigate in-situ ACEO and ACET mixing effect. The electrode-electrolyte interaction was described by lumped circuit model for wide range of ionic strength mediums (1 mS m^{-1} to 1 S m^{-1}). Impedance measurements revealed more capacitive characteristic for low ionic strength fluids and mixing efficiency was enhanced by ACEO secondary flow. The equivalent electric circuit represented more resistive effect by increasing the electrolyte conductivity. Generated temperature gradients in high conductive solutions were used in order to induce ACET force as the secondary flow to facilitate the mixing effects. Concentration distribution revealed a good perturbation effects associated with stretching and folding effects for mixing the fluids with conductivity range varied from 1 mS m^{-1} to 1 S m^{-1}. Mixing quality increased by using more electrode arrays and increasing the amplitude of electric potential.

Conflict of Interest

All authors declare no conflicts of interest in this paper.

Reference

1. Kaajakari V (2009) Practical MEMS: Design of microsystems, accelerometers, gyroscopes, RF MEMS, optical MEMS, and microfluidic systems, Las Vegas, NV: Small Gear Publishing.
2. Vafaie RH, Ghavifekr HB, Lintel HV, et al. (2016) Bi-directional AC electrothermal micropump for on-chip biological applications. *Electrophoresis* 37: 719–726.
3. Poorreza A, Vafaie RH, Mehdipoor M, et al. (2013) A microseparator based-on 4-phase travelling wave dielectrophoresis for Lab-on-a-chip applications. *Indian J Pure Appl Phys* 51: 506–515.
4. Vafaie RH, Mehdipoor M, Pourmand A, et al. (2013) An electroosmotically-driven micromixer modified for high miniaturized microchannels using surface micromachining. *Biotechnol Bioprocess Eng* 18: 594–605.
5. Nguyen NT, Wu Z (2004) Micromixers—a review. *J Micromech Microeng* 15: R1.
6. He B, Burke BJ, Zhang X, et al. (2001) A picoliter-volume mixer for microfluidic analytical systems. *Anal Chem* 73: 1942–1947.
7. Mengeaud V, Josserand J, Girault HH (2002) Mixing processes in a zigzag microchannel: finite element simulationsand optical study. *Anal Chem* 74: 4279–4286.
8. Ryu KS, Shaikh K, Goluch E, et al. (2004) Micro magnetic stir-bar mixer integrated with parylene microfluidic channels. *Lab Chip* 4: 608–613.
9. Yang Z, Matsumoto S, Goto H, et al. (2001) Ultrasonic micromixer for microfluidic systems. *Sensor Actuat A Phys* 93: 266–272.
10. Français O, Jullien MC, Rousseau L, et al. (2007) An active chaotic micromixer integrating thermal actuation associating PDMS and silicon microtechnology. *Arxiv preprint arXiv*: 0711.3290.
11. Morgan H, Green NG (2003) AC electrokinetics: Colloids and nanoparticles, Baldock, Hertfordshire: Research Study Press LTD.

12. Biddiss E, Erickson D, Li D (2004) Heterogeneous surface charge enhanced micromixing for electrokinetic flows. *Anal Chem* 76: 3208–3213.
13. Fu LM, Yang RJ, Lin CH, et al. (2005) A novel microfluidic mixer utilizing electrokinetic driving forces under low switching frequency. *Electrophoresis* 26: 1814–1824.
14. Meisel I, Ehrhard P (2006) Electrically-excited (electroosmotic) flows in microchannels for mixing applications. *Eur J Mech B-Fluid* 25: 491–504.
15. Chen CK, Cho CC (2008) Electrokinetically driven flow mixing utilizing chaotic electric fields. *Microfluid Nanofluid* 5: 785–793.
16. Yang CK, Chang JS, Chao SD, et al. (2007) Two dimensional simulation on immunoassay for a biosensor with applying electrothermal effect. *Appl Phys Lett* 91: 113904.
17. Sigurdson M, Wang D, Meinhart CD (2005) Electrothermal stirring for heterogeneous immunoassays. *Lab Chip* 5: 1366–1373.
18. Huang KR, Chang JS, Chao SD, et al. (2008) Simulation on binding efficiency of immunoassay for a biosensor with applying electrothermal effect. *J Appl Phys* 104: 064702.
19. Ramos A, Morgan H, Green NG, et al. (1998) Ac electrokinetics: a review of forces in microelectrode structures. *J Phys D Appl Phys* 31: 2338.
20. Zhu J, Xuan X (2009) Dielectrophoretic focusing of particles in a microchannel constriction using DC-biased AC flectric fields. *Electrophoresis* 30: 2668–2675.
21. Williams SJ, Green NG (2015) Electrothermal pumping with interdigitated electrodes and resistive heaters. *Electrophoresis* 36: 1681–1689.
22. Vafaie RH, Ghavifekr HB (2017) Configurable ACET micro-manipulator for high conductive mediums by using a novel electrode engineering. *Microsys Technol* 23: 1393–1403.
23. Chang CC, Yang RJ (2004) Computational analysis of electrokinetically driven flow mixing in microchannels with patterned blocks. *J Micromech Microeng* 14: 550.
24. Probstein RF (2005) Physicochemical hydrodynamics: an introduction, John Wiley & Sons.
25. Landau LD, Bell JS, Kearsley MJ, et al. (2013) Electrodynamics of continuous media, Elsevier.
26. Lide DR (2004) CRC handbook of chemistry and physics, CRC press.
27. Yuan Q, Yang K, Wu J (2014) Optimization of planar interdigitated microelectrode array for biofluid transport by AC electrothermal effect. *Microfluid Nanofluid* 16: 167–178.
28. Chen JK, Yang RJ (2007) Electroosmotic flow mixing in zigzag microchannels. *Electrophoresis* 28: 975–983.
29. Taguchi G, Chowdhury S, Wu Y (2005) Taguchi's quality engineering handbook, Wiley.
30. Huang SH, Hsueh HJ, Hung KY (2010) Configurable AC electroosmotic generated in-plane microvortices and pumping flow in microchannels. *Microfluid Nanofluid* 8: 187–195.
31. Jorcin JB, Orazem ME, Pébère N, et al. (2006) CPE analysis by local electrochemical impedance spectroscopy. *Electrochim Acta* 51: 1473–1479.
32. Erickson D, Li D (2002) Influence of surface heterogeneity on electrokinetically driven microfluidic mixing. *Langmuir* 18: 1883–1892.

AIMS Press